

Concomitant polymorphs: structural studies on the trimorphic dithiadiazolyl radical, CICN^{δ+}SSN^{δ-}†

Andrew D. Bond, Delia A. Haynes, Christopher M. Pask and Jeremy M. Rawson*

Department of Chemistry, The University of Cambridge, Lensfield Road, Cambridge, UK CB2 1EW

Received 28th November 2001, Accepted 2nd April 2002
First published as an Advance Article on the web 10th May 2002

The radical CICN^{δ+}SSN^{δ-} (**1**) exhibits a rigid geometry which limits structural variation in the solid state to differences in packing motifs. Sublimation of **1** (75 °C, 10⁻² Torr) leads to the isolation of three distinct polymorphs; **1α** (monoclinic, *P*₂₁/*n*) crystallises as *cisoid* dimers with two molecules in the asymmetric unit, **1β** (monoclinic, *P*₂₁/*c*) crystallises as twisted dimers with four molecules in the asymmetric unit and **1γ** (monoclinic, *P*₂₁/*c*) crystallises as *cisoid* dimers (similar to **1α**), but with eight molecules in the asymmetric unit. Despite their structural variations, all three structures exhibit similar structure-directing motifs based upon electrostatic S^{δ+} ··· N^{δ-} contacts.

The dithiadiazolyl radical, RCN^{δ+}SSN^{δ-}, has been utilised successfully in the construction of molecular conductors and magnets.¹ The materials properties of these radicals are intrinsically linked to their solid-state structure, and a basic understanding of the factors which dictate the crystal structure is necessary if new materials are to be constructed in a pre-defined manner. The effect of polymorphism in this area is clearly illustrated in the case of *p*-NCC₆F₄CN^{δ+}SSN^{δ-}.² This radical crystallises in two morphologies; both morphologies contain chains of molecules linked together through CN^{δ+} ··· S^{δ+} electrostatic interactions. The *α*-phase^{2a} is triclinic *P* $\bar{1}$ with chains arranged antiparallel through an inversion centre, whereas the *β*-phase^{2b} (orthorhombic *Fdd2*) has coparallel chains and is macroscopically polar. Whilst the *β*-phase orders as a weak ferromagnet at 36 K, the *α*-phase orders as an antiferromagnet at low temperatures. A number of other dithiadiazolyl radicals have also been found to be polymorphic.³ The influence of polymorphism on molecular materials has been reviewed recently.⁴ Clearly, the identification of key structure-directing interactions is of importance in the development of these radicals as both molecular conductors and magnets. In the former case, increasing the structural dimensionality of the system has been proposed^{1a} to inhibit Peierls distortions which lead to a transition from metallic to semi-conducting/insulating state. In the latter case, structural control is necessary to develop a three-dimensional network of contacts between radical centres which will lead to the possibility of bulk magnetic order.^{1c}

Complete crystal structure prediction, even for simple molecules, is a complex problem.⁵ One alternative approach has been a detailed study of observed solid-state structures to determine structure-directing motifs. The use of so-called supramolecular synthons (functional groups which give rise to well-defined solid-state interactions) has proved successful at imparting some structural control in molecular crystals. Even so, additional problems, such as polymorphism,⁶ may arise, which clearly indicate that there are several essentially equi-energetic methods of packing molecules in the solid state. Whilst the observation of polymorphism might prove frustrating, a comparison of the structures of these different polymorphs may prove instructive in understanding, in a qualitative

way, the competing intermolecular forces which act during the crystal growth process. Here we report the crystal structures of three concomitant polymorphs (*i.e.* they all crystallise under the same experimental conditions) of a dithiadiazolyl radical, CICN^{δ+}SSN^{δ-} (**1**). Their structures are analysed through an examination of electrostatic interactions using molecular electrostatic potential maps and point charge models.

Experimental

Me₃SiNCNSiMe₃ (Lancaster), SCl₂ (Aldrich) and Zn/Cu couple (Lancaster) were used as supplied. Et₂O was dried over Na wire and SO₂ (Aldrich) dried over P₂O₅ prior to use.

Preparation of 1

Radical **1** was prepared according to the literature method,⁷ and crystals were isolated by vacuum sublimation (75 °C, 10⁻² Torr) to yield a mixture of air-sensitive blue-black blocks and green-black needles.

X-Ray crystallography

Single crystal X-ray diffraction analyses were performed using a Nonius KappaCCD diffractometer equipped with an Oxford Cryosystems cryostream device. In order to handle the air-sensitive crystals without decomposition, samples were opened under a flow of argon gas and transferred directly to perfluoropolyether oil cooled to 270 K under a second cryostream device. Crystals were mounted and transferred immediately to the diffractometer and data were collected at 180(2) K.⁸ Data were processed using the HKL package⁹ and unit-cell parameters were refined against all data (see Table 1).

CCDC reference numbers 175270–175272.

See <http://www.rsc.org/suppdata/dt/b1/b110922g/> for crystallographic data in CIF or other electronic format.

Theoretical calculations

Semi-empirical calculations were made using MOPAC implemented through Quantum Cache (Fujitsu Co.) on the gas phase structures of **1** and HCN^{δ+}SSN^{δ-}. Geometry optimisation using AM1 proved to give superior structural compatibility with that observed experimentally than PM3, and the AM1 method was used in subsequent calculations. The structural parameters for **1**

† Electronic supplementary information (ESI) available: comment on the effect of the basis set on calculated point charges in S/N radicals. See <http://www.rsc.org/suppdata/dt/b1/b110922g/>

Table 1 Crystal data for **1**

	1α	1β	1γ
Empirical formula	CCIN ₂ S ₂	CCIN ₂ S ₂	CCIN ₂ S ₂
Crystal system	Monoclinic	Monoclinic	Monoclinic
Space group	<i>P</i> 2 ₁ / <i>n</i>	<i>P</i> 2 ₁ / <i>c</i>	<i>P</i> 2 ₁ / <i>c</i>
<i>a</i> /Å	9.0394(4)	10.8281(3)	12.3032(2)
<i>b</i> /Å	9.7477(4)	11.7958(5)	21.0874(5)
<i>c</i> /Å	10.1784(5)	14.1753(5)	13.8532(2)
β /°	90.554(2)	91.971(3)	104.022(1)
<i>V</i> /Å ³	896.81(7)	1809.48(11)	3487.01(11)
<i>Z</i>	8	16	32
<i>D</i> _c /g cm ⁻³	2.068	2.050	2.127
Crystal size/mm	0.23 × 0.23 × 0.16	0.21 × 0.07 × 0.05	0.35 × 0.25 × 0.18
Crystal morphology	Block	Needle	Block
Total data	5110	16085	30456
Unique data	2021	4091	7903
<i>R</i> _{int}	0.0330	0.0745	0.0398
<i>R</i> 1 [<i>F</i> ² > 2σ(<i>F</i> ²)]	0.0249	0.0392	0.0286
<i>wR</i> 2 (all data)	0.0658	0.1587	0.0761
Goodness of fit	1.07	1.03	1.10
ρ _{min} , ρ _{max} /e Å ⁻³	-0.552, 0.495	-0.802, 0.703	-0.490, 0.490

Table 2 Optimised geometry and partial charges for **1** and HCNSSN calculated using AM1 and PM3 semi-empirical methods

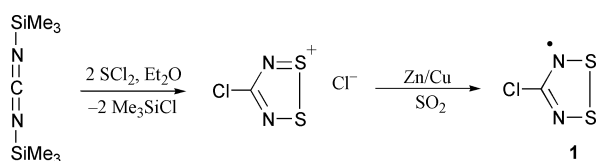
Compound Method	1			HCNSSN		
	Observed	AM1	PM3	Observed	AM1	PM3
Bond lengths/Å						
S–S	2.08 ± 0.01	2.005	2.065	2.07 ± 0.03	2.003	2.059
N–S	1.64 ± 0.01	1.584	1.706	1.64 ± 0.06	1.591	1.711
C–N	1.33 ± 0.01	1.361	1.355	1.32 ± 0.08	1.350	1.347
Cl–C	1.72 ± 0.01	1.704	1.671	—	—	—
H–C	—	—	—	0.95 ^a	1.110	1.099
Bond angles/°						
NSS	94.8 ± 0.05	96.6	94.5	95 ± 3	96.5	94.3
CNS	112.2 ± 0.9	112.7	116.1	113 ± 5	112.3	116.2
NCN	125.7 ± 0.9	121.2	118.8	124.4 ± 4	122.3	118.8
Partial charges						
S	—	+0.24	+0.19	—	+0.23	+0.17
N	—	-0.28	-0.28	—	-0.32	-0.29
C	—	-0.03	-0.04	—	-0.05	+0.05
Cl	—	+0.11	+0.22	—	—	—
H	—	—	—	—	+0.23	+0.17

^a Added at calculated position.

calculated using AM1 and PM3 are given in Table 2. Molecular electrostatic isopotential maps for **1** were determined using AM1 for both the optimised and observed geometries, but showed no significant differences.

Results

Radical **1** was prepared according to the literature method,⁷ from the reaction of Me₃SiNCNSiMe₃ with SCl₂ followed by reduction with Zn/Cu couple in *l.* SO₂ (Scheme 1). Radical **1** is

**Scheme 1**

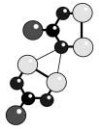

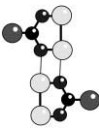
extremely air sensitive. Crystals of **1** were grown by vacuum sublimation (75 °C, 10⁻² Torr) from which two clear morphologies could be identified; lustrous blue–black blocks (**1 α**) and green–black needles (**1 β**). Structural studies indicated that the blocks contained a third polymorph (**1 γ**), which could not be distinguished by inspection from **1 α** .

Structure of **1 α**

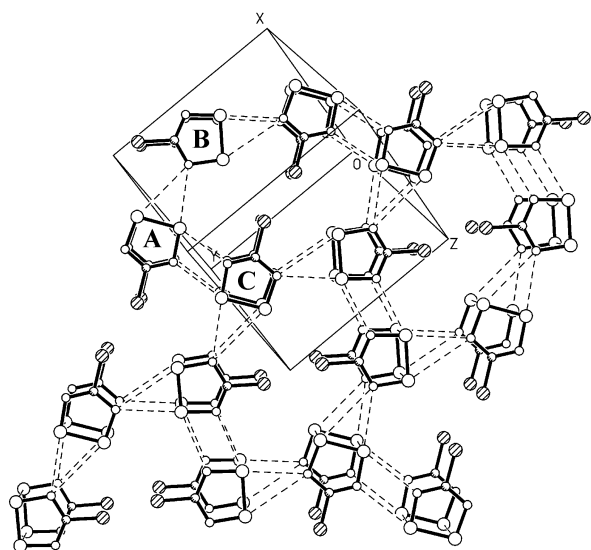
1 α crystallises as a *cisoid* dimer with two molecules in the asymmetric unit. The intramolecular distances are unexceptional and comparable with other dithiadiazolyl radicals.¹⁰ The intra-dimer S...S contacts of 3.004(1) and 3.138(1) Å are comparable to those observed for other dithiadiazolyl radicals.¹⁰ These distances are substantially less than the sum of the van der Waals radii perpendicular to the ring plane¹¹ [4.06 Å] and facilitate the π^* – π^* bonding interaction which renders these dimers diamagnetic in the solid state.¹⁰ The *cis* conformation of the dimer, coupled with the close S...S contact necessarily leads to intra-dimer Cl...Cl contacts [3.585(1) Å] close to the sum of the van der Waals radii (3.56 Å).¹¹ The discrepancy in intra-dimer contacts at S and at Cl is accommodated by the heterocyclic ring planes within the dimer being inclined at 5.7° with respect to each other.

The solid-state packing of these dimeric units comprises layers of molecules close to the (101) plane. Within these layers, there are two different types of S...N contacts. The first links the two S atoms of one dithiadiazolyl ring to a nitrogen of a second ring (dimers **A** and **B** in Fig. 1). The N atom is displaced away from the molecular two-fold axis of the first ring, giving an asymmetric set of S...N contacts (Table 3); the shorter contacts around 3.0 Å are somewhat less than the sum of the

Table 3 Selected intermolecular contacts for the three polymorphic modifications of **1**

	1α	1β	1γ
Intra-dimer S \cdots S	S(11) \cdots S(21) 3.138(1) S(12) \cdots S(22) 3.004(1)	S(11) \cdots S(21) 3.145(2) S(31) \cdots S(41) 3.012(2)	S(11) \cdots S(21) 2.925(1) S(12) \cdots S(22) 3.138(1) S(31) \cdots S(41) 3.147(1) S(32) \cdots S(42) 3.005(1) S(51) \cdots S(61) 2.966(1) S(52) \cdots S(62) 3.156(1) S(71) \cdots S(81) 3.138(1) S(72) \cdots S(82) 2.943(1)
	N(21) \cdots S(11) ^a 3.478(2) N(21) \cdots S(12) ^a 3.011(1) N(11) \cdots S(21) ^a 3.470(2) N(11) \cdots S(22) ^a 3.053(2)	N(12) \cdots S(21) ^b 3.050(4) N(12) \cdots S(22) ^b 3.039(4) N(41) \cdots S(31) ^d 3.217(4) N(41) \cdots S(32) ^d 2.878(4)	N(11) \cdots S(31) ^c 2.885(2) N(11) \cdots S(32) ^c 3.131(2) N(21) \cdots S(41) ^c 2.898(2) N(21) \cdots S(42) ^c 3.046(2) N(31) \cdots S(71) 3.213(2) N(31) \cdots S(72) 3.066(2) N(41) \cdots S(81) 3.383(2) N(41) \cdots S(82) 3.214(2) N(52) \cdots S(11) 3.141(2) N(52) \cdots S(12) 3.332(2) N(62) \cdots S(21) 2.988(2) N(62) \cdots S(22) 3.146(2) N(72) \cdots S(51) 3.113(2) N(72) \cdots S(52) 2.888(2) N(82) \cdots S(61) 3.040(2) N(82) \cdots S(62) 2.844(2)
		N(22) \cdots S(41) ^b 2.886(3) N(22) \cdots S(42) ^b 2.960(4) N(32) \cdots S(11) ^e 2.891(3) N(32) \cdots S(12) ^e 2.910(3)	
	N(12) \cdots S(22) ^f 3.294(1) S(12) \cdots N(22) ^f 3.232(1) N(22) \cdots S(22) ^f 3.082(2)		N(32) ^g \cdots S(61) 3.165(2) N(42) ^g \cdots S(51) 3.097(2) N(51) ^g \cdots S(42) 3.150(2) N(61) ^g \cdots S(32) 3.074(2)
N \cdots Cl	Cl(11) \cdots N(22) ^h 3.388(1)	N(11) \cdots Cl(21) ⁱ 3.102(4)	N(12) \cdots Cl(31) 3.242(2) N(22) \cdots Cl(41) 3.291(2) N(71) \cdots Cl(51) ^e 3.268(2) N(81) \cdots Cl(61) ^e 3.313(2)

^a $3/2 - x, 1/2 + y, 1/2 - z$. ^b $3 - x, -1/2 + y, 1/2 - z$. ^c $-1 + x, y, z$. ^d $4 - x, 2 - y, -z$. ^e $4 - x, 1/2 + y, 1/2 - z$. ^f $2 - x, 1 - y, -z$. ^g $1 - x, -1/2 + y, 5/2 - z$. ^h $1/2 + x, 3/2 - y, 1/2 + z$. ⁱ $3 - x, 1/2 + y, 1/2 - z$.

**Fig. 1** Crystal structure of **1 α** viewed close to the (101) plane, illustrating the layer-like arrangement of molecules.

van der Waals radii [3.20 Å]¹¹ whilst the longer contacts (*ca.* 3.4–3.5 Å) are a little longer than the sum of the van der Waals radii. The second set of S \cdots N interactions correspond to the

location of dimer pairs around an inversion centre, leading to an antiparallel alignment of dimers (**A** and **C**). These contacts (*ca.* 3.2 Å, Table 3) are also close to the sum of the van der Waals radii. Other in-plane contacts lie beyond the sum of the van der Waals radii for in-plane contacts;¹¹ the Cl \cdots Cl and S \cdots Cl distances between dimers are around 3.3 and 3.5 Å, respectively [*cf.* the sums of the van der Waals radii at 3.16 and 3.18 Å for Cl \cdots Cl and S \cdots Cl, respectively].

Between these layers, the dimers are approximately stacked around the inter-dimer C \cdots C vector with rotations alternating between +120 and –120° down the stacking direction (Fig. 2). This leads to inter-dimer Cl \cdots N contacts of 3.388(1) and 3.610(2) Å, similar to, or greater than, the sum of the van der Waals radii perpendicular to the ring plane¹¹ [3.38 Å]. In addition, there are inter-stack S \cdots S contacts between dithiadiazolyl radicals. This centrosymmetric interaction is similar in geometry to the $\pi^*-\pi^*$ bonding interaction observed in [S₃N₂]₂²⁺ salts,¹² although the S \cdots S contacts in **1 α** are considerably longer. The shortest of these is S(21) \cdots S(22)[2 – *x*, 1 – *y*, 1 – *z*] at 3.763(1) Å, which is a little less than the sum of the van der Waals radii of S perpendicular to the ring plane¹¹ [4.06 Å].

Structure of **1 β**

The asymmetric unit of **1 β** comprises two crystallographically independent $\pi^*-\pi^*$ dimers which adopt a twisted configuration,

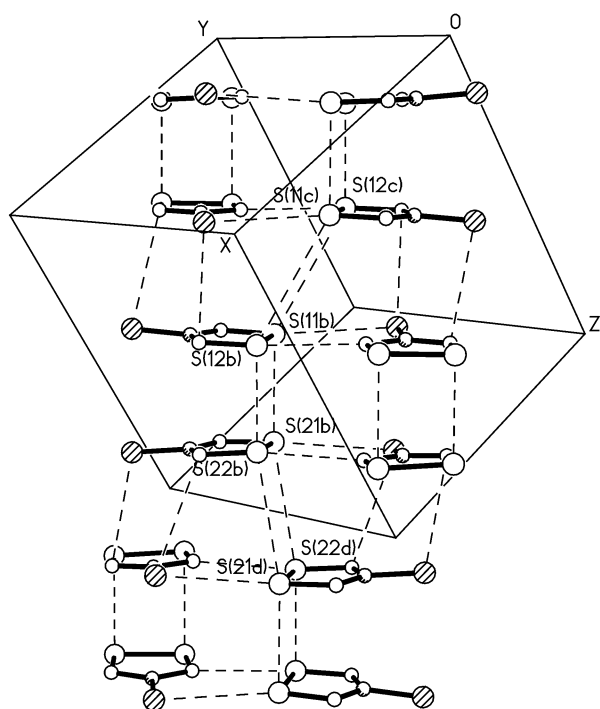


Fig. 2 Crystal structure of **1a** viewed perpendicular to the molecular layers.

with molecules linked through a single S...S contact [S(11) ... S(21) 3.145(2) and S(31) ... S(41) 3.012(2) Å]. Twisted $\pi^*-\pi^*$ dimers have previously been reported¹³ for CF_3CNSSN , Me_2NCNSSN , MeCNSSN , $2,3\text{-F}_2\text{C}_6\text{H}_3\text{CNSSN}$ and the adamantyl derivative, AdCNSSN . The lack of Cl...Cl contact in the twisted dimer configuration allows the two heterocyclic rings within the dimers to reside closer to planarity than observed in **1a** (and **1 γ**); the angles between heterocyclic mean planes are 2.4 and 4.8° for the two independent dimers. In the following discussion, the two crystallographically distinct dimers will be referred to as **A** and **B**.

The packing of **1 β** is more complex than the structure of **1a** (and also **1 γ**). In **1a** and **1 γ** , a layer-like structure is observed, with the molecular plane approximately coincident with the layers. In **1 β** , there are two crystallographically independent sheets, lying in the *yz* plane (see Figs. 3 and 4).

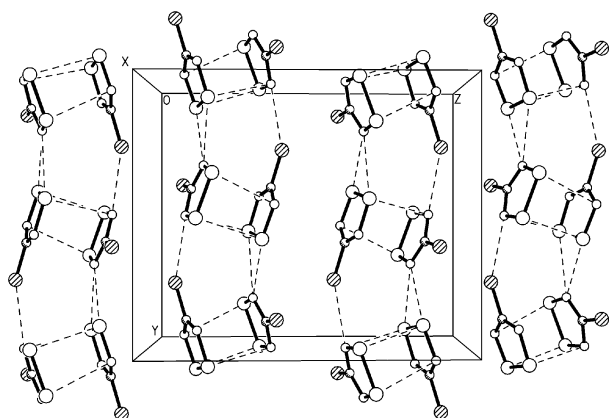


Fig. 3 View of the crystal structure of **1 β** in the *yz* plane, showing the layer-like nature of one of the two crystallographically unique dimers (**A**).

The first layer comprises dimers of **A**. Within this layer, the heterocyclic ring planes lie approximately perpendicular to the *yz* plane. Dimers are linked *via* short S...N contacts, similar

to those observed in **1a** between the disulfur bridge and the N of the next dimer. In the β -phase, they are considerably shorter [*ca.* 3.0 Å (see Table 3)] and more symmetric than those observed in **1a**. These contacts link dimers into infinite chains along the crystallographic *y* axis. There are additional N...Cl contacts [N(11) ... Cl(2) 3.102(4) Å] close to the sum of the van der Waals radii¹¹ [3.18 Å].

The second layer comprises dimers of **B** (see Fig. 4). These

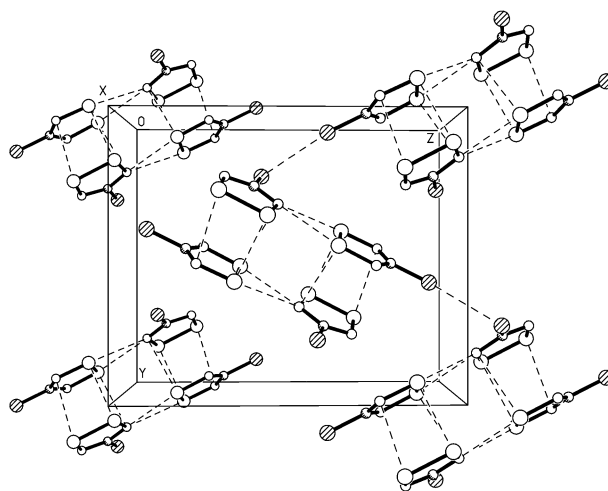


Fig. 4 View of the crystal structure of **1 β** in the *yz* plane, showing the layer-like nature of the second crystallographically unique dimer (**B**).

dimers associate through pairs of S...N contacts similar to those described above, but which form discrete centrosymmetric tetramers; the S...N contacts are more asymmetric than those observed in the first layer and shorter than those observed in **1a**, ranging from *ca.* 2.9 to 3.2 Å.

The layers of **A** and **B** dimers are connected *via* further S...N contacts between the disulfur bridges of one layer and the N atoms of the next layer (Fig. 5). The intermolecular

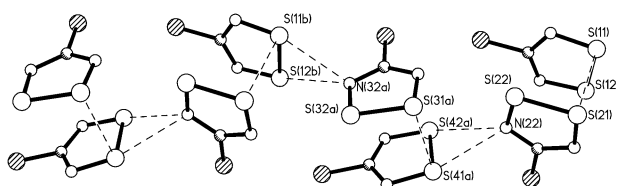


Fig. 5 View of the crystal structure of **1 β** , illustrating the inter-layer interactions.

contacts are similar to the in-layer contacts described above, with approximately symmetric S...N contacts around 2.9 Å (Table 3). However, whereas the S...N interactions within the layers lie close to the molecular plane (as in **1a** and **1 γ**), these inter-layer contacts show a substantial twist between the two heterocyclic rings involved, such that the two rings are almost mutually perpendicular. The angle between the mean plane of molecules **1** and **3** is 91.8°, and between **2** and **4** it is 91.7°.

Structure of **1 γ**

The asymmetric unit of **1 γ** comprises four crystallographically independent dimers, which all exhibit a *cisoid* configuration, analogous to **1a**. These four dimers are hereafter referred to as **A–D**. The molecular and intra-dimer geometries are similar to those observed for **1a**: *e.g.* the intra-dimer S...S contacts [2.925(1) to 3.156(1) Å (Table 3)] are similar to those observed for **1a**. The Cl...Cl contacts range from 3.500(1) to 3.566(1) Å. The angle between ring planes in each dimer fall into two groups; dimers **A** and **D** possess angles of 8.6 and 8.4°, respec-

tively; the remaining two dimers (**B** and **C**) exhibit more acute angles of 5.4 and 5.7°, respectively.

The packing of **1 γ** resembles that of **1 α** in that it possesses a layer-like structure with the molecular plane lying close to the plane of the layer (Fig. 6). The *cisoid* dimers in **1 γ** are linked in

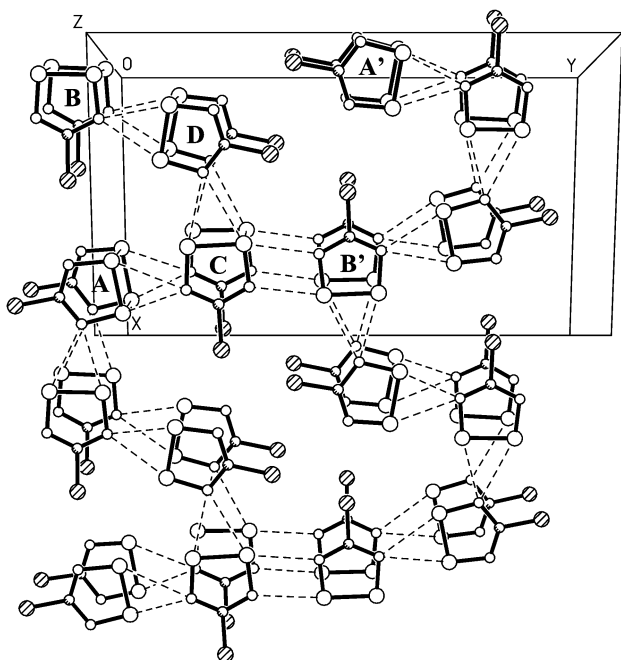


Fig. 6 Crystal structure of **1 γ** in the *xy* plane, illustrating the layer-like arrangement of molecules.

the molecular plane *via* similar sets of S...N interactions to those observed in **1 α** , but generate different packing motifs. In **1 γ** , the disulfur bridge of one molecule interacts with a unique N of a second molecule forming chains along the *x* axis. These S...N contacts are considerably shorter than those observed in **1 α** , but still exhibit some asymmetry with a long and short S...N contact. The spread of observed intermolecular S...N distances for the 8 independent molecules is quite large, so that there is considerable overlap between the 'long' and 'short' contacts which each molecule makes. The shorter contacts range from 2.844(2) to 3.214(2) Å (Table 3), whereas the longer distances fall in the region 3.046(2) to 3.383(2) Å. The structure of **1 γ** also exhibits lateral sets of S...N contacts (e.g. **B'**...**C** in Fig. 6) analogous to **1 α** , which link dimers along the crystallographic *y* axis. These too are shorter (Table 3) than those observed in **1 α** , and a little shorter than the sum of the van der Waals radii, around 3.1 Å.¹¹

The packing of **1 γ** perpendicular to the *xy* plane comprises stacking of dimers with an intra-dimer separation of *ca.* 4.0 Å. Three distinct stacking patterns are observed: one stack contains dimers **A** and **B**, a second stack contains dimer **C**, and a third stack contains dimer **D** (see Fig. 7). The dimers **A** and **B** form a stacked motif along *z* with dimers **A** and **B** related by rotation by ~90° along *z*. This inter-dimer geometry is reminiscent of that observed in **1 β** , although the shortest of these inter-dimer S...S contacts [S(42b)...S(21a) 3.924(1) Å] are considerably longer than the intra-dimer S...S contacts observed in **1 β** [3.012(2)–3.145(2) Å]. The dimer **C** forms a slipped π -stack of cofacially aligned dimers with inter-dimer S...S contacts [S(51b)...S(62a) 4.009(1) and S(52b)...S(61a) 4.028(1) Å] near to the sum of the van der Waals radii. The slipped nature of the π -stack leads to closer inter-dimer S...N contacts [S(52b)...N(61a) 3.579(2) and S(51b)...N(62a) 3.644(2) Å], also close to the sum of the van der Waals radii. The fourth dimer, **D**, stacks with an approximately antiparallel alignment of the C–N bonds, generating

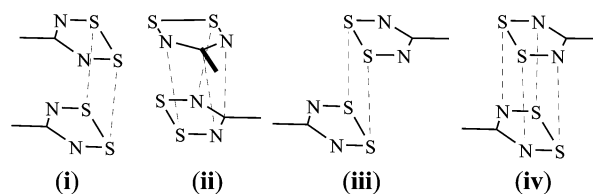
S...Cl contacts between dimers, again close to the sum of the van der Waals radii; Cl(7a)...S(82c) 3.538(1) and S(7a)...Cl(8c) 3.680(1) Å.

Relative polymorph stability

A number of analytical methods are available for determining the relative stabilities of different polymorphs.⁶ The very air-sensitive nature of **1**, however, coupled with the similar appearances of **1 α** and **1 γ** , has precluded Pasteur separation of different polymorphs of **1** for analysis by DSC and other methods. Whilst there are some exceptions, the density rule¹⁴ has proved a convenient method of predicting the relative stabilities of polymorphs. It assumes that the most efficient packing motif (with the highest density) will have maximised the lattice energy. On this basis, the stability of the polymorphs is in the order **1 γ** > **1 α** ~ **1 β** .

Discussion

In the majority of cases, dithiadiazolyl radicals associate as $\pi^*-\pi^*$ *cisoid* dimers (i),¹⁰ giving rise to a closed-shell electronic configuration, although a diverse variety of other modes of association are possible,^{13,15} which facilitate this $\pi^*-\pi^*$ bonding interaction (ii–iv). Solution EPR studies indicate that the enthalpy of dimerisation is substantial (*ca.* 35 kJ mol⁻¹).¹⁶ Theoretical calculations support the observation that dimerisation is enthalpically favourable, although the exact value of the dimerisation energy is sensitive to the basis set employed.¹⁷ Additional calculations have indicated that the energetic difference between the different conformers is very small.^{13a} Whilst a number of monomeric dithiadiazolyl radicals have been reported in recent years,^{2,15b,18} the vast majority are dimeric in the solid state, which is consistent with this large dimerisation energy.



Whilst a few empirical models have been developed¹⁹ to understand the gross solid-state structures of these radicals, no substantial attempts have been made, as far as we are aware, to rationalise the structures of these radicals. In order to do so, simple derivatives, XCNSSN, appear to be good models since these are rigid planar molecules. The simplest derivative, HCNSSN, has been reported previously^{17,20} and has been found to crystallise in two forms; a monoclinic phase¹⁷ (*P*₂*1*/*n*) and a triclinic phase²⁰ (*P* $\bar{1}$). In the latter case, a channel-like structure is formed with nitrogen included within the channels. Here we assess the observed structural motifs in both **1** and HCNSSN in terms of electrostatic interactions.

Molecular electrostatic potential map

Semi-empirical calculations on **1** and HCNSSN were made using AM1 and PM3 methods. Both AM1 and PM3 methods provided satisfactory estimates of molecular geometry and also wavefunctions in good agreement with those determined previously.^{13a,17,21} In addition, s and p orbital unpaired spin densities were in good agreement with those estimated from EPR studies of dithiadiazolyl radicals.²² The charge distributions in both cases were also similar. Of the two methods, AM1 was chosen for the determination of the molecular electrostatic potential (MEP) maps, since it provided a better reproduction

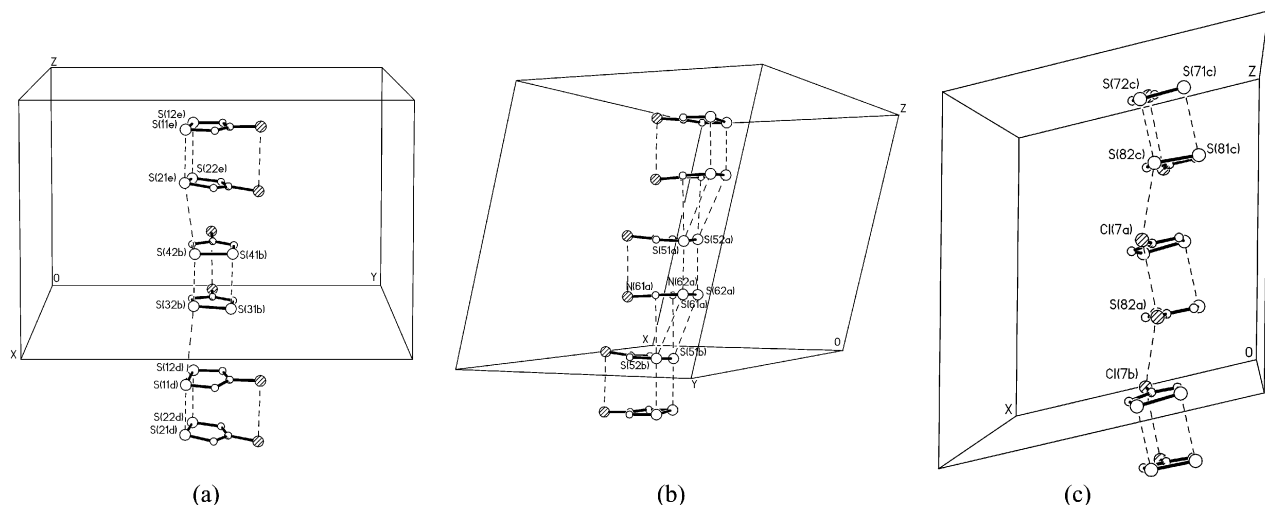


Fig. 7 Views of the packing of molecules in **1** γ ; (a) dimers **A** and **B** form twisted π -stacks; (b) dimer **C** forms slipped *cisoid* π -stacks; and (c) dimer **D** does not exhibit a π -stacking motif.

of the experimental geometry.[‡] (The MEPs derived from the PM3 wavefunction were not substantially different from those calculated using the AM1 function, nor were MEPs determined using the AM1 wavefunction and the experimental geometry.)

The molecular electrostatic potential may be more revealing than the atomic point charges.²³ The MEP is the energy associated with a unit positive point charge ('a proton') and the unperturbed molecular charge distribution, caused by the electrons and positive nuclei. The isopotential map represents a contour linking points with the same interaction energy. The energy may be positive if the MEP at that point is repulsive, or negative if the sum of the electrostatic interactions is attractive.²⁴ The molecular electrostatic isopotential surface shown in Fig. 8(a) represents an energy surface around a molecule of

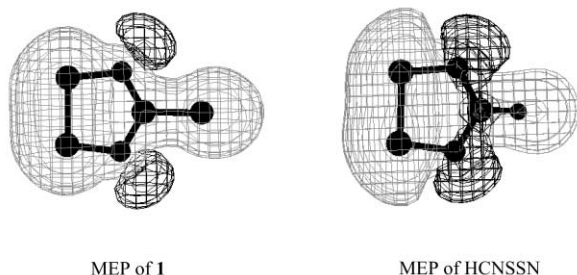


Fig. 8 Molecular electrostatic isopotential maps of (a) **1** and (b) HCNSSN calculated at 0.04 au.

1 such that black-lined regions indicate a negative, attractive potential for a positive charge and grey-lined regions are repulsive.

A large number of dithiadiazolyl radicals form π -stacked motifs in the solid state. Along the π -stacking direction, the bonding is complex; π -bonding interactions, dispersion forces and electrostatic interactions may contribute to the total energy. However, perpendicular to the stacking direction, the interactions may be considered to be predominantly dispersive and

electrostatic in nature. The dispersion forces are non-directional and merely favour close-packing of molecules, whereas the electrostatic contribution is very directional and is optimised by matching of partial positive and negative charges. An examination of the MEP surface may therefore provide a useful method for analysing the solid-state structures of these dithiadiazolyl radicals perpendicular to the π -stacking direction.

The MEP map of **1** [Fig. 8(a)] clearly shows that net positive potentials are found near the S and Cl atoms, whilst there are negative potentials close to the N atoms, in agreement with the point charges (Table 3). In a purely electrostatic model, the energy will be optimised with efficient matching of the black and grey regions of the MEP. In the case of **1**, packing motifs which optimise particularly S \cdots N and, to a lesser extent, Cl \cdots N will be favourable. If we now analyse the structures of **1** in terms of the possible combinations of energetically favourable interactions, we observe very good agreement between the MEP and the structural motifs. These are described below.

Sulfur–nitrogen contacts

We focus on S \cdots N interactions in the first instance, since these are likely to be a recurrent theme in dithiadiazolyl structures. Since the S and N atoms bear the greatest partial positive and negative charges (at the AM1 level), the S \cdots N contacts may be anticipated to dominate over Cl \cdots N contacts in an electrostatic model. An analysis of the MEP of **1** shows three favourable in-plane combinations of matching S \cdots N contacts. These are shown in Fig. 9. Some combination of these favourable interactions is likely to occur in the structures of dithiadiazolyl radicals, although these may be affected by both the steric and electrostatic properties of the substituent.

The motif SN-I is apparent in all the structures of **1**, although there is a clearly observable asymmetry in the interaction, characterised by longer S \cdots N contacts to the S atom which makes a close approach to Cl. This asymmetry can be thought to arise through electrostatic S ^{$\delta+$} \cdots Cl ^{$\delta+$} repulsions. This SN-I interaction is also seen in other dithiadiazolyl structures, such as HCNSSN²⁰ (see later) and CF₃CNSSN.^{13a} Because the interactions are electrostatic, there is no necessity for the two heterocyclic rings to be co-planar and an SN-I' geometry with a torsion angle between ring planes is also possible, as observed in **1** β . Here, minimisation of steric effects produces a more symmetric set of S \cdots N contacts. Evidently, the steric requirements of the substituent will play an important role in the final geometry of this contact. In many instances,

[‡] PM3 gives slightly larger positive partial charges on Cl than S and so would predict enhanced Cl \cdots N interactions in preference to S \cdots N. As these are not observed, this gives additional support to the choice of AM1 as our basis set. It also infers that an appropriate choice of basis set is necessary to reproduce and rationalise molecular interactions. Studies on the related system F₃CCNSCCF₃ at higher levels of calculation have indicated substantial variation in calculated point charges, despite good geometric agreement between calculated and observed structures. Semi-empirical calculations on the same molecule gave a similar distribution of point charges. These data are available as ESI.

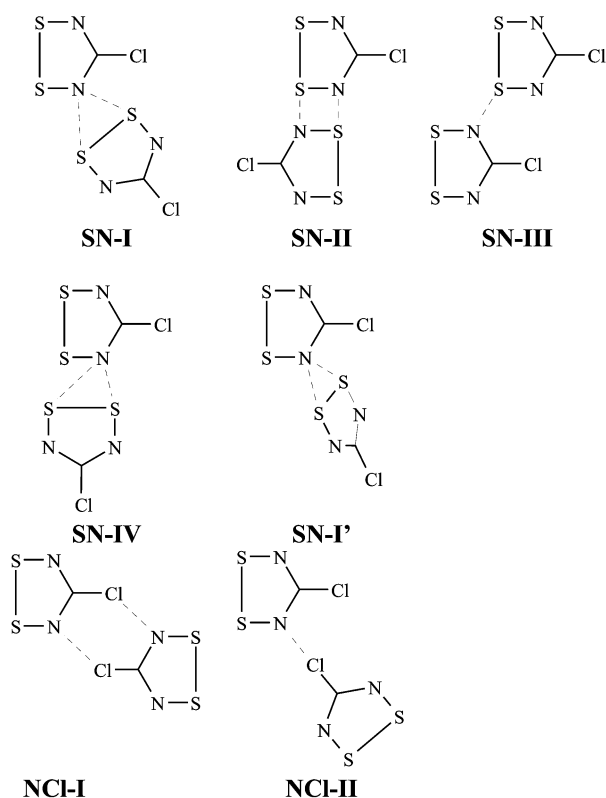


Fig. 9 Electrostatically favourable $S \cdots N$ and $N \cdots Cl$ contacts expected for **1**.

especially with aromatic substituents, this SN-I geometry is likely to deform and the modified geometry SN-IV would be common, although probably less favoured than SN-I. This SN-IV interaction occurs,^{13b,25} for example, in $Me_2NCNSSN$, $NSSNCCNSSN$, $1,3,5-C_6H_3(CNSSN)_3$, $2,5-F_2C_6H_3CNSSN$ ^{13e} and $3,5-F_2C_6H_3CNSSN$.²⁶ The loss in electrostatic $S^{\delta+} \cdots N^{\delta-}$ interaction, and increased $S^{\delta+} \cdots S^{\delta+}$ repulsion may be partially balanced by a greater dispersion term between S atoms. Indeed, a continuum of steps can be envisaged between the two interactions. The angle formed between the two molecular two-fold axes provides a convenient measure of the deformation between SN-I ($\theta \approx 60^\circ$)[§] and SN-IV ($\theta \approx 90^\circ$). In the case of **1**, these angles vary; in **1a** $\theta \approx 73^\circ$, whereas in **1γ**, it more closely resembles SN-IV, with θ ranging from 76 to 82° .

The antiparallel interaction SN-II provides a pair of favourable $S \cdots N$ contacts, like SN-I, and, because of the minimisation of steric repulsions, is less susceptible to modification by substituents. This motif appears in both **1a** and **1γ**. It occurs extensively in planar derivatives with aryl substituents, e.g. in $p-NCC_6H_4CNSSN$,^{15a} $m-NCC_6H_4CNSSN$,^{15a} $p-ClC_6H_4CNSSN$,²⁷ $3,5-(NC)_2C_6H_3CNSSN$ ²⁷ and $3,4-F_2C_6H_3CNSSN$,²⁶ as well as the charge-transfer salts $[p-C_6H_4(CNSSN)_2]X$ ($X = Br, I$).^{18e,28}

The interaction SN-III is less common, exhibiting only one $S \cdots N$ interaction between radicals. Nevertheless, there is the possibility of forming multiple interactions of this type, since it requires only one S or N atom from each ring to form the interaction. Whilst not present in any of the polymorphs of **1**, it occurs, for example, in the β -phase of $p-NCC_6F_4CNSSN$ ^{2b} and $p-C_6H_4(CNSSN)_2$,²⁹ in the former case, each dithiadiazolyl ring forms four such contacts. It also occurs in the charge transfer salt $[(CNSSN)_2]I$.³⁰

In all cases, the $S \cdots N$ contacts in all three polymorphs of **1** [Table 2] are close to, or less than, the sum of the in-plane van

der Waals radii [*ca.* 3.2 Å], with shortening of the contacts caused by the favourable electrostatic interaction.

Contacts involving Cl

The substituent on the dithiadiazolyl ring will have important steric and electronic contributions to the structure of the dithiadiazolyl radical. In the current case, the electropositive nature of the Cl favours $N \cdots Cl$ contacts. Two favourable contacts are anticipated; the antiparallel geometry NCI-I, with two interactions per radical pair, or NCI-II, with only one $N \cdots Cl$ interaction per radical pair. An examination of the structures of **1** reveals very few close $Cl \cdots N$ contacts equal to or less than the sum of the van der Waals radii [*ca.* 3.2 Å].¹¹ This indicates that they are energetically less favourable than the plethora of $S \cdots N$ contacts described above. Of the close contacts observed, only one is less than the sum of the van der Waals radii; in **1β**, there is an intermolecular $N \cdots Cl$ contact at 3.102(4) Å [$N(11) \cdots Cl(21)$, related *via* the symmetry operator: $3-x, 1/2 + y, 1/2 - z$]. A close $N \cdots Cl$ contact approximately equal to the sum of the van der Waals radii is also seen in **1γ** at 3.268(2) Å [$N(71) \cdots Cl(51)$ related *via* the symmetry operator $-1 + x, y, z$]. Since electrostatic interactions fall off as r^{-1} , then contacts beyond the sum of the van der Waals radii may still be favourable, although the paucity of close $Cl \cdots N$ contacts clearly indicate that they have a less structure-directing influence than the $S \cdots N$ contacts.

Competing interactions

The observation of polymorphism in **1** indicates that combinations of these interactions lead to structures with similar lattice energies. The complex web of short $S^{\delta+} \cdots N^{\delta-}$ contacts and the absence of close $Cl^{\delta+} \cdots N^{\delta-}$ contacts indicates that the $S^{\delta+} \cdots N^{\delta-}$ interactions play a key role in determining the solid-state structure in **1**. The two phases of the *cisoid* dimer, **1a** and **1γ**, are particularly instructive in determining the possible methods of packing. In both cases, a layer-like structure is formed, within which each dimer has eight near neighbours, arranged in a distorted grid structure. The 'corner' molecules are more distant and we focus on the interactions to the four nearest-neighbour molecules.

In the case of **1a**, three of the four contacts fall within the sum of the van der Waals radii and comprise two SN-I contacts and an SN-II interaction. The fourth appears as a longer $Cl \cdots Cl$ contact (attractive in terms of dispersion forces, but electrostatically repulsive). In the case of **1γ**, there are four dimers in the asymmetric unit. Here, there are two distinct environments; in the first environment, dimers **B** and **C** (Fig. 6) take up geometries with two type SN-I and one SN-II interaction. The fourth interaction is a long $N \cdots Cl$ contact. The other two dimers (**A** and **D**, Fig. 6) in **1γ** take up geometries exhibiting two SN-I interactions, plus additional $N \cdots Cl$ contacts, beyond the sum of the van der Waals radii. The structure of **1β**, whilst different in the mode of association, also exhibits two SN-I contacts per radical. Given the similar stabilities of **1a**, **1β** and **1γ** (all form under identical conditions) we suggest that this SN-I interaction is strongly structure-directing.

We can formulate two of the different polymorphs of **1** (**1a** and **1γ**) as arising from the propagation of these SN-I/SN-IV interactions, illustrated schematically in Fig. 10. Both **1a** and **1γ** originate from the same packing motif, but addition of the third *cisoid* dimer can occur in one of two orientations. In **1a**, propagation of these contacts through an 'all-trans' orientation generates a herring-bone motif, whereas in **1γ**, an alternating *cis-trans* pattern generates an alternative polymeric structure. It is notable that another alternative packing derived from these $S \cdots N$ contacts is not observed (**1δ**), *i.e.* discrete cyclic tetramers (or larger oligomers, *cf.* HCNSSN discussed below). This pin-wheel motif has been observed in other derivatives, such as $2,5-F_2C_6H_3CNSSN$.^{13e}

§ If we assume that the optimised angle for an SN-I interaction requires the two-fold axis of one molecule to be coincident with the N angle bisector, then this angle for **1** is $61 \pm 1^\circ$.

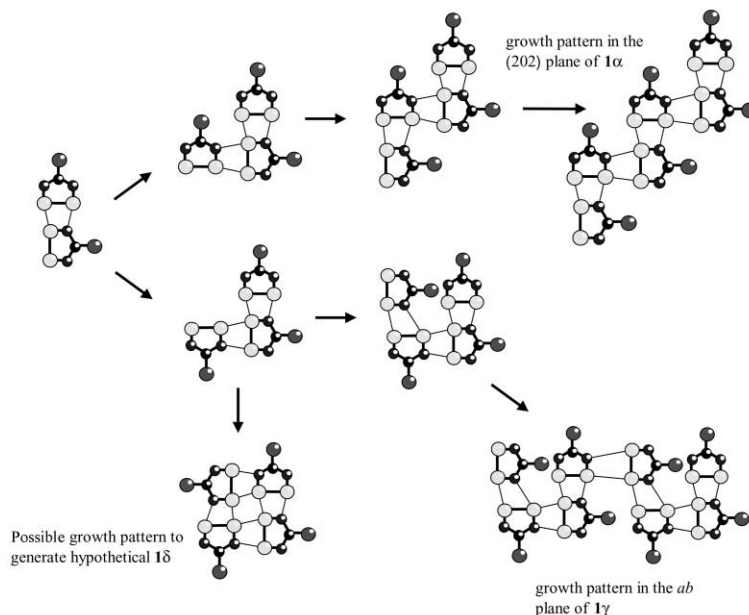


Fig. 10 Development of different growth patterns of **1** using SN-IV interactions (Fig. 9) in the molecular plane. This approach generates a hypothetical **1δ** structure, as well as the observed structures of **1α** and **1γ**. The optimised geometry is intermediate between SN-I and SN-IV and the observed structures of **1α** and **1γ** are slightly distorted from these packing motifs to accommodate this optimised geometry.

Geometric minima

The prediction of polymorphs is an area of chemistry still in its infancy.⁵ The problem requires the summation of all the dispersion, electrostatic and any other contributions to the lattice energy, and depends on the space group, the unit-cell dimensions and molecular orientation. With increasing numbers of molecules in the asymmetric unit, the problem becomes, at best, computationally expensive and, at worst, impossible.⁵ Given the problems with structure prediction for even the most simple of systems (one rigid molecule in the asymmetric unit), attempts to predict the solid-state structure of ClCNSSN were not attempted. Instead, we have searched for local minima in the modes of association of radical pairs in the molecular plane in the gas phase. A methodology was employed which summed the dispersion and electrostatic contributions to the interatomic, intermolecular interactions in a pairwise fashion, *i.e.* the “atom–atom approach”.³¹ A Lennard-Jones [6–12] potential³² was used to describe the dispersion forces, with the minimum of the well set to be equal to the sum of the van der Waals radii. The depth of the potential well (ϵ) was less easy to define. An empirical correlation³³ between atomic polarisability (α)³⁴ and the depth of the potential well was observed for the inert gases [Ne, Ar and Xe]:

$$\epsilon(K) = 50r_{\text{vdw}}\sqrt{\alpha} \quad (1)$$

A similar atom–atom dispersion term was applied to all atoms, and an arbitrary scaling factor included. The magnitude of the scaling factor seemed to have little influence on the resultant geometry (close-packed with intermolecular distances close to the sum of the van der Waals radii), but evidently had a profound influence on the total energy of the system. The electrostatic contribution was calculated with a simple point charge model,³² using partial atomic charges determined from the semi-empirical AM1 methods.

Geometry optimisation of radical pairs starting from 8 different positions (in which the second molecule is located at 45° intervals around the first molecule) yielded four local energy minima, which are depicted in Fig. 11. The two lowest energy minima correspond closely to the observed $S^{\delta+} \cdots N^{\delta-}$ contacts in the structures of **1**, specifically SN-I and SN-II. The coulombic contributions to these minima are substantial, particularly in comparison to those involving Cl \cdots N inter-

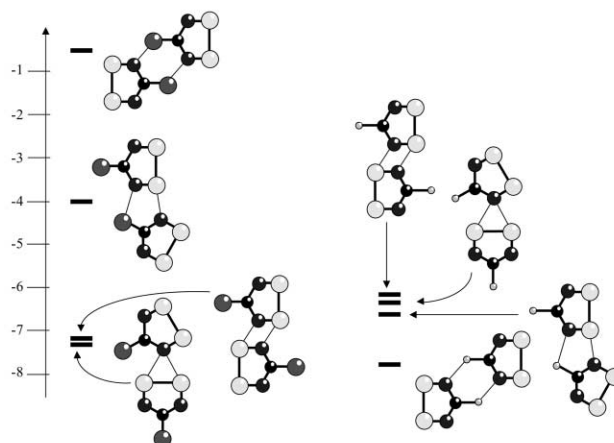


Fig. 11 Calculated electrostatic energies (kJ mol^{-1}) for in-plane interactions in **1** and HCNSSN, using point charges determined from semi-empirical MOPAC/AM1 methods.

actions. The latter are calculated to be coulombically 4–7 kJ mol^{-1} less stable and this may rationalise the apparent absence of close $N \cdots Cl$ contacts observed in all three polymorphs of **1**. The calculated intermolecular contacts in SN-I and SN-II geometries are in good agreement with the experimental data (3–4% error) and also replicate the asymmetry in the interaction in SN-I. In the case of SN-I, the optimised angle was 68° (*cf.* 73–82° observed in **1α** and **1γ**). Whilst this discrepancy may be due to deficiencies in the potential energy model, we do not discount perturbations in the observed geometry caused by packing effects. The broad agreement not only in the relative strengths of the intermolecular interactions, but also in the observed and calculated geometries is gratifying and augers well for the application of this methodology to more extended structures rather than dimer pairs. In order to check the validity of the approach, we have extended it to the simple derivative HCNSSN.

Analysis of the structure of HCNSSN

The structure of HCNSSN was reported by Oakley and co-workers in 1993.¹⁷ It crystallises in the space group $P2_1/n$, with three crystallographically independent *cisoid* dimers in the

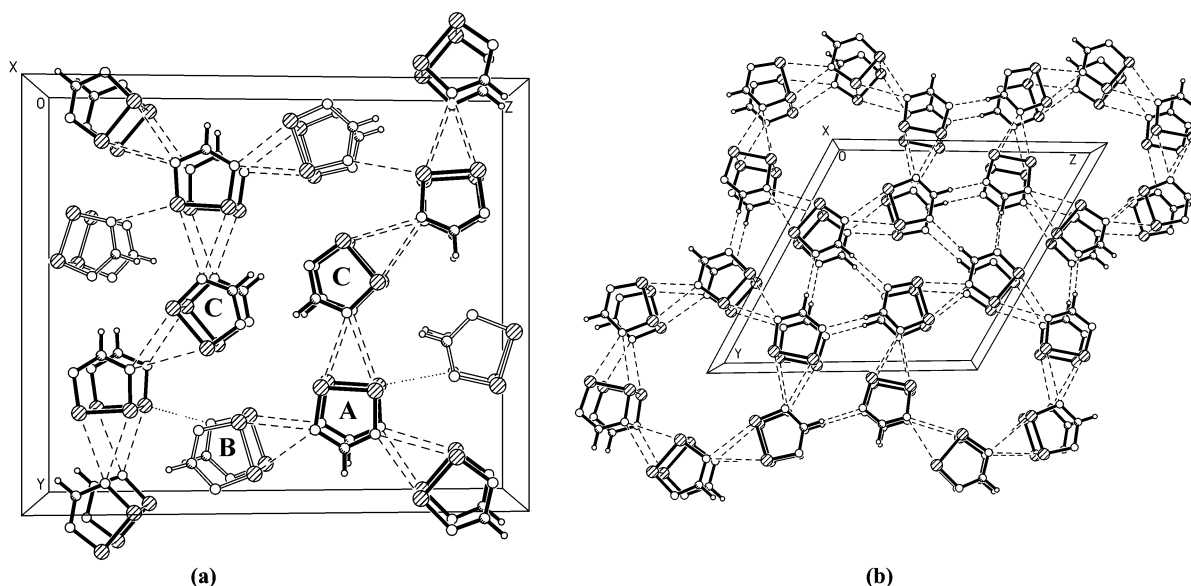


Fig. 12 Crystal structures of HCNSSN,^{17,20} illustrating both the SN-I and C–H \cdots N interactions present in these structures.

asymmetric unit. A second, triclinic, phase ($P\bar{1}$) was reported²⁰ in 1994, which is formed along with the original monoclinic phase. This second phase also contains three *cisoid* dimers in the asymmetric unit and crystallises with nitrogen included in a channel-like structure. The structures of both phases are shown in Fig. 12.

We employed the same electrostatic approach to analyse the packing in HCNSSN as that used in **1**; *i.e.* an initial study of the molecular electrostatic potential, followed by a simple optimisation of the in-plane interactions within a pair of radicals, utilising calculated point charges.

The MEP map for HCNSSN is shown in Fig. 8 and closely resembles that for **1**, indicating a likely preference for S \cdots N contacts. The partial charges indicate that the H atom exhibits a larger partial positive charge than the Cl atom in **1**. Indeed, the similarity in partial charge on both H and S means that competition between H \cdots N and S \cdots N contacts is possible.

Calculations of favourable gas phase in-plane interactions yield qualitatively similar optimised geometries as those determined for **1**, although the relative energies of these interactions differ. The calculated coulombic interactions in all four geometry-optimised minima are identical within 1.5 kJ mol⁻¹. Most notably, the symmetric C–H \cdots N ‘hydrogen-bonding’ interaction is substantially more favourable than the Cl \cdots N interactions in **1** (Fig. 11), and is expected to be competitive with the SN-I type interaction. The optimised geometry for the latter is more symmetric than that for **1** ($\theta = 54^\circ$) and presumably arises from the minimal steric bulk of the H atom in contrast to Cl.

The observed packing of both phases of HCNSSN reflect the favourable SN-I type electrostatic interaction, as well as a propensity for N \cdots H contacts. In both phases, each molecule forms an average of two SN-I type contacts (analogous to **1**). There is good agreement between the observed (58–61°) and calculated ($\theta = 54^\circ$) angles between the two molecular C₂ axes. In the monoclinic phase, two of the crystallographically independent dimers [A and C in Fig. 12(a)] form a ribbon-like structure along the *y* axis (shown in bold in Fig. 12a), linked *via* pairs of SN-I interactions. One of these dimers (A) forms a third SN-I contact to a pendant radical (B) which is not part of the chain. B itself only forms one SN-I contact, but has additional favourable C–H \cdots N and S \cdots N contacts. Additional C–H \cdots N contacts (between C and C') link chains together in a centrosymmetric fashion. The triclinic phase exhibits approximate hexagonal geometry, with molecules linked *via* a pair of SN-I interactions to form discrete hexamers.

Each molecule now has only five nearest neighbours, with included nitrogen located in the ‘vacant’ channel. Each molecule in the hexagon is linked to two additional hexagons *via* N \cdots H contacts through non-crystallographic three-fold symmetry in the triclinic phase.

Conclusion

The observation of concomitant polymorphism in **1** arises through different, but energetically similar, modes of packing. Theoretical calculations indicate that whilst a substantial contribution to the energy of the in-plane interactions arises from dispersion forces, electrostatic interactions between molecules may play a key role in dictating the packing motifs. An analysis of these favourable electrostatic interactions may prove useful in the design of molecular materials based on these radicals. The current studies on **1** and HCNSSN indicate that SN-I type interactions are important in determining their structures. The observation of multiple polymorphs in both **1** and HCNSSN indicates that the prediction of solid-state structures is likely to be complicated by multiple crystal structures of similar energy. Whilst this may appear disheartening, this observation also means that many new polymorphs may be awaiting discovery subject to adjustment of the crystallisation conditions.

Acknowledgements

We would like to thank the EPSRC (A. D. B., C. M. P.) and the Cambridge Commonwealth Trust (D. A. H.) for financial support.

References and notes

- (a) A. W. Cordes, R. C. Haddon and R. T. Oakley, *Adv. Mater.*, 1994, **6**, 798; (b) A. W. Cordes, R. C. Haddon and R. T. Oakley, in *The Chemistry of Inorganic Ring Systems*, ed. R. Steudel, Elsevier, Amsterdam, 1992; (c) J. M. Rawson and F. Palacio, in *π -Electron Magnetism: From Molecules to Magnetic Materials*, ed. J. Veciana, Springer-Verlag, Berlin, 2001; (d) G. Antorrena, F. Palacio, J. M. Rawson and J. N. B. Smith, in *Supramolecular Engineering of Synthetic Metallic Materials: Conductors and Magnets*, NATO-ASI Ser., Ser. C, Kluwer Academic, Dordrecht, 1998, vol. 518, p. 217.
- (a) A. J. Banister, N. Bricklebank, W. Clegg, M. R. J. Elsegood, C. I. Gregory, I. Lavender, J. M. Rawson and B. K. Tanner, *J. Chem. Soc., Chem. Commun.*, 1995, 679; (b) A. J. Banister, N. Bricklebank, I. Lavender, J. M. Rawson, C. I. Gregory, B. K. Tanner, W. Clegg, M. R. J. Elsegood and F. Palacio, *Angew. Chem., Int. Ed Engl.*, 1996, **35**, 2533.

- 3 A. W. Cordes, R. C. Haddon, R. G. Hicks, R. T. Oakley and T. T. M. Palstra, *Inorg. Chem.*, 1992, **31**, 1802.
- 4 J. S. Miller, *Adv. Mater.*, 1998, **10**, 1553.
- 5 (a) P. Verwer and F. J. J. Leusen, in *Reviews in Computational Chemistry*, ed. K. B. Lipkowitz and D. B. Boyd, Wiley-VCH, New York, 1988, ch. 7, p. 12; (b) J. P. M. Lommerse, W. D. S. Motherwell, H. L. Ammon, J. D. Dunitz, A. Gavezzotti, D. W. M. Hofmann, F. J. J. Leusen, W. T. M. Mooij, S. L. Price, B. Schweizer, M. U. Schmidt, B. P. van Eijck, P. Verwer and D. E. Williams, *Acta Crystallogr., Sect. B*, 2000, **56**, 697.
- 6 (a) J. Bernstein, R. G. Davey and J.-O. Henck, *Angew. Chem., Int. Ed.*, 1999, **38**, 3440; (b) J. D. Dunitz and J. Bernstein, *Acc. Chem. Res.*, 1995, **28**, 193.
- 7 H.-U. Höfs, R. Mews, W. Clegg, M. Noltemeyer, M. Schmidt and G. M. Sheldrick, *Chem. Ber.*, 1983, **116**, 416.
- 8 COLLECT, Nonius B. V., Delft, The Netherlands, 1998.
- 9 Z. Otwinski and W. Minor, *Methods Enzymol.*, 1997, **276**, 307.
- 10 J. M. Rawson, A. J. Banister and I. Lavender, *Adv. Heterocycl. Chem.*, 1995, **62**, 137.
- 11 S. C. Nyburg and C. H. Faerman, *Acta Crystallogr., Sect. B*, 1985, **41**, 274.
- 12 (a) B. Krebs, G. Henkel, S. Pohl and H. W. Roesky, *Chem. Ber.*, 1980, **113**, 226; (b) R. Gleiter, R. Bartetzko and P. Hoffmann, *Z. Naturforsch., B*, 1980, **35**, 1166; (c) R. J. Gillespie, J. P. Kent and J. F. Sawyer, *Inorg. Chem.*, 1981, **20**, 3784; (d) U. Thewalt and M. Burger, *Z. Naturforsch., B*, 1981, **36**, 293; (e) R. W. H. Small, A. J. Banister and Z. V. Hauptman, *J. Chem. Soc., Dalton Trans.*, 1984, 1377; (f) B. Ayres, A. J. Banister, P. D. Coates, M. I. Hansford, J. M. Rawson, C. E. F. Rickard, M. B. Hursthouse, K. M. A. Malik and M. Motevalli, *J. Chem. Soc., Dalton Trans.*, 1992, 3097.
- 13 (a) H. U. Hofs, J. W. Bats, R. Gleiter, G. Hartmann, R. Mews, M. Eckert-Maksic, H. Oberhammer and G. M. Sheldrick, *Chem. Ber.*, 1985, **118**, 3781; (b) A. W. Cordes, J. D. Goddard, R. T. Oakley and N. P. C. Westwood, *J. Am. Chem. Soc.*, 1989, **111**, 6147; (c) A. J. Banister, M. I. Hansford, Z. V. Hauptman, S. T. Wait and W. Clegg, *J. Chem. Soc., Dalton Trans.*, 1989, 1705; (d) J. N. Bridson, S. B. Copp, M. J. Schriver, Z. Shuguang and M. Zawarotko, *Can. J. Chem.*, 1994, **72**, 1143; (e) A. J. Banister, A. S. Batsanov, O. G. Dawe, P. L. Herbertson, J. A. K. Howard, S. Lynn, I. May, J. N. B. Smith, J. M. Rawson, T. E. Rogers, B. K. Tanner, G. Antorrena and F. Palacio, *Chem. Commun.*, 1997, 2539.
- 14 A. Burger and R. Ramberger, *Mikrochim. Acta*, 1979, **2**, 259.
- 15 (a) A. W. Cordes, R. C. Haddon, R. G. Hicks, R. T. Oakley and T. T. M. Palstra, *Inorg. Chem.*, 1992, **31**, 1802; (b) T. M. Barclay, A. W. Cordes, N. A. George, R. C. Haddon, M. E. Itkis and R. T. Oakley, *Chem. Commun.*, 1999, 2269; (c) N. Bricklebank, S. Hargreaves and S. E. Spey, *Polyhedron*, 2000, **19**, 1163.
- 16 (a) N. Burford, J. Passmore and M. J. Schriver, *J. Chem. Soc., Chem. Commun.*, 1986, 140; (b) W. V. F. Brooks, N. Burford, J. Passmore, M. J. Schriver and L. H. Sutcliffe, *J. Chem. Soc., Chem. Commun.*, 1987, 69; (c) S. A. Fairhurst, K. M. Johnson, L. H. Sutcliffe, K. F. Preston, A. J. Banister, Z. V. Hauptman and J. Passmore, *J. Chem. Soc., Dalton Trans.*, 1986, 1465.
- 17 A. W. Cordes, C. D. Bryan, W. M. Davis, R. H. de Laat, S. H. Glarum, J. D. Goddard, R. C. Haddon, R. G. Hicks, D. K. Kennepohl, R. T. Oakley, S. R. Scott and N. P. C. Westwood, *J. Am. Chem. Soc.*, 1993, **115**, 7232.
- 18 (a) G. Antorrena, J. E. Davies, M. Hartley, F. Palacio, J. M. Rawson, J. N. B. Smith and A. Steiner, *Chem. Commun.*, 1999, 1393; (b) C. M. Pask, R. J. Less, J. M. Rawson, F. Palacio and P. Oliete, *Phosphorus, Sulfur Silicon Relat. Elem.*, 2001, **168**, 457; (c) R. A. Beeckman, R. T. Boere, K. H. Moock and M. Parvez, *Can. J. Chem.*, 1998, **76**, 85; (d) A. J. Banister, I. Lavender, J. M. Rawson, W. Clegg, B. K. Tanner and R. J. Whitehead, *J. Chem. Soc., Dalton Trans.*, 1993, 1421; (e) C. D. Bryan, A. W. Cordes, R. M. Fleming, N. A. George, S. H. Glarum, R. C. Haddon, C. D. MacKinnon, R. T. Oakley, T. T. M. Palstra and A. S. Perel, *J. Am. Chem. Soc.*, 1995, **117**, 6880.
- 19 (a) J. M. Rawson, R. J. Less, J. N. B. Smith, F. Palacio and G. Antorrena, *Mol. Cryst. Liq. Cryst.*, 1999, **334**, 275; (b) J. M. Rawson, R. J. Less, C. M. Pask, J. E. Davies, A. E. Goeta, J. A. K. Howard, F. Palacio and P. Oliete, manuscript in preparation.
- 20 C. D. Bryan, A. W. Cordes, R. C. Haddon, R. G. Hicks, D. K. Kennepohl, C. D. MacKinnon, R. T. Oakley, T. T. M. Palstra, A. S. Perel, S. R. Scott, L. F. Schneemeyer and J. V. Waszczak, *J. Am. Chem. Soc.*, 1994, **116**, 1205.
- 21 P. J. Alonso, G. Antorrena, J. I. Martinez, J. J. Novoa, F. Palacio, J. M. Rawson and J. N. B. Smith, *Appl. Magn. Reson.*, 2001, **20**, 231.
- 22 J. M. Rawson, A. J. Banister and I. May, *Magn. Reson. Chem.*, 1994, **32**, 487.
- 23 *Computational Chemistry*, ed. G. H. Grant and W. G. Richards, *Oxford Chemistry Primer*, Oxford University Press, London, 1996, p. 29.
- 24 Quantum Cache version 5.0, On-Line Manual, Fujitsu Co., Tokyo, Japan, 2001.
- 25 (a) A. W. Cordes, R. C. Haddon, R. G. Hicks, R. T. Oakley, T. T. M. Palstra, L. F. Schneemeyer and J. V. Waszczak, *J. Am. Chem. Soc.*, 1992, **114**, 5000; (b) C. D. Bryan, A. W. Cordes, R. C. Haddon, R. G. Hicks, R. T. Oakley, T. T. M. Palstra and A. J. Perel, *J. Chem. Soc., Chem. Commun.*, 1994, 1447.
- 26 A. J. Banister, A. S. Batsanov, O. G. Dawe, J. A. K. Howard, J. E. Davies, J. M. Rawson and J. N. B. Smith, *Phosphorus, Sulfur Silicon Relat. Elem.*, 1997, **124/5**, 553.
- 27 (a) W. M. Davis, R. G. Hicks, R. T. Oakley, B. Zhao and N. J. Taylor, *Can. J. Chem.*, 1993, **71**, 180; (b) R. T. Boere, K. H. Moock and M. Parvez, *Z. Anorg. Allg. Chem.*, 1994, **620**, 1589.
- 28 C. D. Bryan, A. W. Cordes, R. M. Fleming, N. A. George, S. H. Glarum, R. C. Haddon, R. T. Oakley, T. T. M. Palstra, A. S. Perel, L. F. Schneemeyer and J. V. Waszczak, *Nature*, 1993, **365**, 821.
- 29 A. W. Cordes, R. C. Haddon, R. T. Oakley, L. F. Schneemeyer, J. V. Waszczak, K. M. Young and N. M. Zimmerman, *J. Am. Chem. Soc.*, 1991, **113**, 582.
- 30 C. D. Bryan, A. W. Cordes, J. D. Goddard, R. C. Haddon, R. G. Hicks, C. D. MacKinnon, R. C. Mawhinney, R. T. Oakley, T. T. M. Palstra and A. S. Perel, *J. Am. Chem. Soc.*, 1996, **118**, 330.
- 31 *The Atom-Atom Potential Method*, ed. A. J. Pertsin and A. I. Kitaigorodski, Springer Verlag, Berlin, 1987.
- 32 P. W. Atkins, *Physical Chemistry*, Oxford University Press, London, 2nd edn., 1984.
- 33 The empirical correlation between the van der Waals radius and atomic polarisability yielded ϵ values for the depth of the potential well (ϵ) of 50, 127 and 218 K for Ne, Ar and Xe, respectively. These provide a qualitative value for ϵ which is comparable with the experimental results (ref. 32) of 36, 124 and 229 K, respectively. The current studies indicate that this needs some modification if it is to reproduce polyatomic systems with better accuracy. In the current study, the optimised geometries of **1** fall very near the sum of the van der Waals radii and the spread of values is much smaller than that observed, indicating that the depth of the potential well is being substantially over-estimated.
- 34 *CRC Handbook of Chemistry and Physics*, Ed. in Chief D. R. Lide, CRC Press, London, 73rd edn., 1993.